Changes in presynaptic gene expression during homeostatic compensation at a central synapse

Abbreviated title: Trans-synaptic regulation of gene expression

Evan R. Harrell[1,2,*], Diogo Pimentel[1], Gero Miesenböck[1,*]

[1] Centre for Neural Circuits and Behaviour, University of Oxford, Tinsley Building, Mansfield Road, Oxford, OX1 3SR, United Kingdom.

[2] Present address: Institute Pasteur, INSERM, Hearing Institute, 63 rue de Charenton, F-75012 Paris, France.

* evan-richard.harrell@pasteur.fr, gero.miesenboeck@cncb.ox.ac.uk

24 pages of text; 5 Figures; 12 Tables.

Word counts: abstract 204; introduction 542; discussion 1657

Acknowledgments: This work was supported by grants from the Wellcome Trust (106988/Z/15/Z, 090309/Z/09/Z, 089270/Z/09/Z) and the Gatsby Charitable Foundation (GAT3237). Paul Overton provided advice on RNA isolation; Amélie Baud gave many helpful tips for the gene ontology analysis; Ruth Brain assisted with stock maintenance and dissections; and Jessica Beevers helped with dissections and made delicious fly food (from the flies' perspective).

Declaration of Interests: The authors declare no competing financial interests.

Abstract

Homeostatic matching of pre- and postsynaptic function has been observed in many species and neural structures, but whether transcriptional changes contribute to this form of trans-synaptic coordination remains unknown. To identify genes whose expression is altered in presynaptic neurons as a result of perturbing postsynaptic excitability, we applied a transcriptomics-friendly, temperature-inducible Kir2.1-based activity clamp at the first synaptic relay of the *Drosophila* olfactory system, a central synapse known to exhibit trans-synaptic homeostatic matching. Twelve hours after adult-onset suppression of activity in postsynaptic antennal lobe projection neurons, we detected changes in the expression of many genes in the third antennal segment, which houses the somata of presynaptic olfactory receptor neurons. These changes affected genes with roles in synaptic vesicle release and synaptic remodeling, including several genes implicated in homeostatic plasticity at the neuromuscular junction. At 48 hours and beyond, the transcriptional landscape was tilted toward proteostasis, energy metabolism, and cellular stress defenses, indicating that the system had been pushed to its homeostatic limits. Our data provide insights into the nature of homeostatic compensation at a central synapse and identify many genes engaged in synaptic homeostasis. The presynaptic transcriptional response to genetically targeted postsynaptic perturbations could be exploited for the construction of novel connectivity tracing tools.

Significance Statement

Homeostatic feedback mechanisms adjust intrinsic and synaptic properties of neurons to keep their average activity levels constant. We show that, at a central synapse in the fruit fly brain, these mechanisms include changes in presynaptic gene expression that are instructed by an abrupt loss of postsynaptic excitability. The trans-synaptically regulated genes have roles in synaptic vesicle release and synapse remodeling; protein synthesis, folding, and degradation; and energy metabolism. Our analysis suggests that similar homeostatic machinery operates at peripheral and central synapses, identifies some of its components, and potentially opens new opportunities for the development of connectivity-based gene expression systems.

Introduction

Homeostatic feedback that stabilizes network activity after synaptic weight changes is an important adjunct to correlation-based learning rules (Turrigiano, 2011). Early demonstrations of homeostatic plasticity followed pharmacological manipulations of synaptic transmission in neuronal cultures (Turrigiano et al., 1994, 1998). When global activity levels were artificially increased or decreased, homeostatic forces intervened to maintain firing rates within defined ranges. These homeostatic forces are generated by two processes (Turrigiano, 2011): cell-autonomous changes in intrinsic excitability, which alter the gain of the neuronal voltage response to synaptic currents (Turrigiano et al., 1994; Desai et al., 1999); and adjustments of the synaptic strengths themselves (Petersen et al., 1997; Davis et al., 1998; Turrigiano et al., 1998; Burrone et al., 2002). These adjustments, though in principle also achievable in a cell-autonomous fashion by altering the density of neurotransmitter receptors in the postsynaptic membrane (Wierenga et al., 2005; Goold and Nicoll, 2010), often involve a trans-synaptic partnership in which postsynaptic neurons communicate deviations from their activity setpoint via retrograde signals to their presynaptic partners, which in turn increase or decrease transmitter release (Cull-Candy et al., 1980; Petersen et al., 1997; Sandrock et al., 1997; Davis et al., 1998; Burrone et al., 2002; Haghighi et al., 2003; Thiagarajan et al., 2005).

Much existing knowledge of retrograde communication comes from studies of the neuromuscular junction (NMJ). In mammals and *Drosophila*, mutations or autoantibodies that reduce the responsiveness of muscle to neurotransmitter cause compensatory increases in motor neuron vesicular release (Cull-Candy et al., 1980; Petersen et al., 1997; Sandrock et al., 1997; Davis et al., 1998). At the *Drosophila* NMJ, acute pharmacological receptor blockade (Frank et al., 2006) or expression of the inwardly rectifying potassium channel Kir2.1 in muscle (Paradis et al., 2001) induce similar presynaptic compensatory effects. While many

gene products and signaling pathways have been implicated in synaptic homeostasis (Davis and Müller, 2015), knowledge of the transcriptional changes that may be required to lock the presynaptic cells into their altered functional state remains scant (Marie et al., 2010).

Pre- and postsynaptic function are also matched at the central synapses between olfactory receptor neurons (ORNs) and projection neurons (PNs) in the antennal lobe of *Drosophila* (Kazama and Wilson, 2008), where the axons of 20–200 ORNs expressing the same odorant receptor connect to dendrites of an average of three affine PNs in a precise anatomical register (Groschner and Miesenböck, 2019). There is clear covariation between the dendritic arbor sizes of PNs belonging to different transmission channels and the amplitudes of unitary excitatory postsynaptic currents (EPSCs): the larger unitary EPSCs of PNs with larger dendritic trees—and, therefore, lower impedances—reflect homeostatic increases in the number of presynaptic ORN release sites in response to increased postsynaptic demand for synaptic drive (Kazama and Wilson, 2008; Mosca and Luo, 2014). This central model of synaptic homeostasis has been characterized physiologically and anatomically, but the molecular mechanisms of synaptic matching are unexplored. Taking advantage of the ease with which the presynaptic partners at this synapse can be isolated (they reside in an external appendage, the third antennal segment), we carried out a transcriptome-wide screen for genes regulated by retrograde homeostatic signals. Homeostatic plasticity was induced by adult-onset expression of Kir2.1 in PNs; the expression of a non-conducting mutant of Kir2.1 (Kir2.1-nc) served as control.

Methods

Drosophila strains and culture

Flies were maintained at 21°C and 65% humidity on a constant 12:12-hour light:dark (LD) cycle in rich cornmeal and molasses-based food with brewer's yeast. Driver lines *GH146-GAL4* (Stocker et al., 1997) and *pdf-GAL4* (Renn et al., 1999) were used to target the expression of codon-optimized *UAS-Kir2.1* transgenes (see below) to PNs and PDF-expressing clock neurons, respectively. Three copies of two *tubulin-GAL80^{ts}* insertions on different chromosomes (McGuire et al., 2003) were combined to achieve tight repression of the GAL4-responsive transgenes until induction. The induction incubator was kept at 31°C in 70% humidity on the same 12:12 LD schedule.

The cDNA sequence encoding human Kir2.1 was codon-optimized for *Drosophila* (GenBank accession number MW088713), synthesized at MWG Eurofins, and fused to a codon-optimized N-terminal EGFP tag. The non-conducting variant (Kir2.1-nc) was created by mutating codon 146 of the ion channel sequence from glycine to serine (GGA to AGC) (Haruna et al., 2007). The channel constructs replaced the mCD8::GFP coding sequence in derivatives of plasmid *pJFRC2-10XUAS-IVS-mCD8::GFP* (Pfeiffer et al., 2010), which were inserted into the *attp2* landing site on the third autosome.

Confocal microscopy

Female flies aged 5 days were anesthetized on ice and dissected in phosphate-buffered saline (PBS; 1.86 mM NaH_2PO_4, 8.41 mM Na_2HPO_4, 175 mM NaCl). Immediately after dissection, brains were fixed in ice-cold PBS containing 4% (w/v) paraformaldehyde for 1–2 hours at room temperature, rinsed three times in ice-cold PBS containing 0.1% (w/v) Triton X-100

(PBT), washed three times for 20 minutes in ice-cold PBT, and mounted and cleared in Vectashield (Vector Labs). Confocal image stacks with an axial spacing of 1–1.5 µm were collected on a Leica TCS SP5 microscope with an HCX IRAPO L 25x/0.95 W objective.

Electrophysiology

Targeted whole-cell patch-clamp recordings from the fluorescent somata of PNs expressing EGFP::Kir2.1 or EGFP::Kir2.1-nc were obtained through a small cranial window in 5-day old females. The brain was continuously superfused with extracellular solution containing 103 mM NaCl, 3 mM KCl, 5 mM TES, 8 mM trehalose, 10 mM glucose, 7 mM sucrose, 26 mM $NaHCO_3$, 1 mM NaH_2PO_4, 1.5 mM $CaCl_2$, 4 mM $MgCl_2$ (pH 7.3) and equilibrated with 95% O_2–5% CO_2. Borosilicate glass electrodes (7–13 MΩ) were filled with intracellular solution containing 140 mM potassium aspartate, 10 mM HEPES, 1 mM KCl, 4 mM Mg-ATP, 0.5 mM Na_3GTP, 1 mM EGTA (pH 7.3). Signals were acquired with a MultiClamp 700B Microelectrode Amplifier, filtered at 6–10 kHz, and digitized at 10–20 kHz with an ITC-18 data acquisition board controlled by the Nclamp and NeuroMatic packages. Data were analyzed with NeuroMatic (http://neuromatic.thinkrandom.com) and custom procedures in Igor Pro (WaveMetrics) (Donlea et al., 2014). The membrane time constant was determined by fitting a single exponential to the voltage deflection caused by a 200-ms-long hyperpolarizing current pulse. Input resistances were estimated from linear fits of the subthreshold voltage deflections elicited by small current pulses of increasing amplitude and a duration of 1 s. Firing rates were quantified by holding cells at resting potentials of –60 ± 2 mV and injecting sequences of depolarizing current pulses (5 pA increments, 1 s duration). Spikes were detected by finding minima in the second derivative of the membrane potential record. The spike rate was calculated by dividing the number of action potentials discharged by the time elapsed between the first and last spike. The current amplitude at which each cell

reached a given frequency threshold (1–50 Hz) was used to construct cumulative distribution functions. The distributions were fit with logistic Naka-Rushton functions of the form (Donlea et al., 2014):

$$F = F_{max} \frac{I^n}{I^n + EC_{50}^n}$$

where F is the percentage of cells reaching threshold at a given current level I, F_{max} is the percentage of cells reaching threshold at maximal current, EC_{50} indicates the half-maximal or semisaturation current, and the exponent n determines the steepness of the curve. With only two free parameters (EC_{50} and n, given that F_{max} is measured experimentally), this simple model provided a satisfying fit to all distributions.

Analysis of circadian behavior

Three-day old female flies were individually inserted into 65 mm glass tubes and loaded into the Trikinetics Drosophila Activity Monitor system, which was operated at 31°C in 24-hour dark (DD) conditions for 5–7 days. Group sizes for activity measurements (16 experimental and 16 control flies) reflect the capacity of the monitors.

Third antennal segment dissection

Groups of 20–30 flies were aged in precisely controlled temperature conditions for 5 days (see Fig. 4*A*) and decapitated with a surgical scalpel on a CO_2 pad; the heads were transferred to petri dishes kept on dry ice. Once a petri dish contained ~50 heads, it was sealed with parafilm and stored at -80°C until RNA extraction. The sealed petri dishes were dipped in liquid nitrogen for 60 seconds, vortexed at full strength for 60 seconds, and then unsealed and placed on a dry-ice-chilled glass stand under a dissection microscope. Individual third antennal segments were picked with fine forceps and placed directly into 100 µl TRIzol (Thermo Fisher Scientific).

177

178 **RNA extraction**

179 Third antennal segments in 100 µl TRIzol were disrupted with several strokes in a Dounce
180 homogenizer. The homogenates were diluted with 900 µl TRIzol and incubated at room
181 temperature for 5 minutes. Samples destined for 3' digital gene expression profiling (3' DGE)
182 underwent phase separation after the addition of 225 µl chloroform; RNA in the aqueous
183 phase was precipitated with isopropanol and resuspended in 5 µl RNase-free water. Total
184 RNA for RNA-seq and RT-qPCR was isolated with the help of RNeasy minelute columns
185 (Qiagen), following the addition of 400 µl of 70% RNase-free ethanol to the TRIzol
186 homogenates and on-column DNaseI digests. Samples were snap frozen in liquid nitrogen and
187 stored at –80°C.

188

189 **cDNA library generation**

190 Libraries for 3’ DGE were generated at MWG Eurofins Genomics from ultrasonically
191 fragmented poly(A)-tailed RNA, which was isolated using oligo(dT) chromatography.
192 Following ligation of an RNA adapter to the 5’-end, the mRNA fragments were reverse-
193 transcribed from an oligo(dT) primer, and the resulting cDNA was PCR-amplified with a
194 high-fidelity polymerase. Each cDNA library was purified, size selected, quality-checked by
195 capillary electrophoresis, and sequenced on the HiSeq2000 platform (Illumina) in 1x100 bp
196 run mode.

197

198 For RNA-seq and RT-qPCR, oligo(dT)-enriched RNA underwent 14 cycles of amplification
199 using the SMARTer Ultra Low RNA Kit for Illumina Sequencing (Clontech). After cDNA
200 fragmentation, libraries were prepared in an additional 15 amplification cycles using the

NEBNext Ultra DNA Library Prep Kit for Illumina (New England Biolabs) and sequenced on the HiSeq2000 platform (Illumina) in paired-end mode.

Transcriptome analysis

Raw reads were 100 base pairs (bp) in length (paired-end reads for RNA-seq and single-ended reads for 3' DGE). Fastq files, containing reads and quality scores, were first run through the FastQC package (Andrews, 2010). Highly abundant sequences that did not map to the *Drosophila* genome (and originated from primers or amplification artefacts) were eliminated using Trimmomatic software (Bolger et al., 2014). Reads were scanned with a 4-bp sliding window and cut when the average quality dropped below 15; trimmed reads shorter than 25 bp were discarded. The reads were mapped to Ensembl DM genome release 5.74 using TopHat2 (Kim et al., 2013), assigned to transcripts annotated in the transcript file of the Berkeley Drosophila Genome Project (BDGP) release 5.74 with Cufflinks, and merged into an experiment-wide gtf file with Cuffmerge (Trapnell et al., 2012). The gtf file was used to produce raw read counts (using HTSeq) suitable for differential expression analysis in DESeq2 (Love et al., 2014). The topGO and *ViSEAGO* packages were used to analyze the enrichment of gene ontology (GO) terms in the set of differentially expressed genes called by DESeq2 (unadjusted $p < 0.05$) vis-à-vis a reference set of all genes with a normalized expression level above 1 (the "gene universe") (Alexa et al., 2006; Brionne et al., 2019). To keep the number of Fisher's exact tests to a minimum, only GO terms with more than 40 attached genes were considered. Enriched GO terms with unadjusted $p < 0.01$ were clustered hierarchically according to Wang's distance, a measure of semantic similarity (Wang et al., 2007; Brionne et al., 2019).

Real time quantitative PCR (RT-qPCR)

Transcript levels were determined by quantitative real-time PCR on a LightCycler 480 system (Roche) using SYBR Green I Master Mix (Roche) in 10-µl reactions containing 100 nM of each gene-specific primer and 50 ng of pre-amplified cDNA. Two sets of primers were designed for each gene of interest. All samples were run in technical triplicates; non-reverse-transcribed mRNA and water served as negative controls. Melting curves were analyzed after amplification, and amplicons were visualized by agarose gel electrophoresis to confirm primer specificity. Relative transcript levels were estimated with the help of the $2^{-\Delta\Delta Ct}$ method (Livak and Schmittgen, 2001), using the housekeeping gene *CycK* for normalization.

Results

Antennal transcriptomics

To characterize gene expression in the third antennal segment, 5-day old male Canton-S (CS) flies were decapitated either between zeitgeber time (ZT) 5 and ZT8 (the day group) or between ZT17 and ZT20 (the night group). After snap-freezing, third antennal segments were manually isolated, and total RNA was extracted in a single batch to minimize variability (Fig. 1*A*, see Methods). For both day and night conditions, three biological replicates were prepared, and the resulting six cDNA libraries were sequenced on one lane of an Illumina HiSeq2000 machine using 3' digital gene expression profiling (3' DGE) technology. After stringent quality assessment and read trimming (Fig. 1*A*), the high-quality reads were mapped to the *Drosophila* genome (for mapping statistics, see Table 1). Biological replicates showed high correlations with one another **(**Fig. 1*B*, Table 1), and day and night samples could easily be distinguished on the basis of their top two principal components (Fig. 1*B*, inset). Underlying this clean separability were 128 differentially expressed genes, identified by DESeq2 (Love et al., 2014) with a false discovery rate (FDR)-adjusted significance level of < 0.2, and large expression level differences between the day and night (Fig. 1*C*, Table 2). Core clock components, such as *cryptochrome*, *Clock*, *period*, *timeless,* and *vrille*, were found near the top of the amplitude distribution of oscillating transcripts (Fig. 1*C*), in two groups at opposite poles of the 24-hour cycle, consistent with their antagonistic roles in the transcriptional feedback oscillator (Claridge-Chang et al., 2001; McDonald and Rosbash, 2001).

Transcripts encoding olfactory, gustatory, and ionotropic receptors (ORs, GRs, and IRs) provided an index of the purity of our library preparations. Certain ORs, IRs, and GRs are

expressed in antennal ORNs but not elsewhere, while others are absent from antennal ORNs but present in different types of sensory neuron (Clyne et al., 1999; Gao and Chess, 1999; Vosshall et al., 1999; Scott et al., 2001; Benton et al., 2009). We detected the former, but not the latter, members of all three receptor families in abundance (Fig. 2*A–C*).

Transcriptomics-friendly manipulation of postsynaptic excitability

Kir2.1 is an inwardly rectifying potassium channel that decreases the input resistance of neurons and clamps their membrane potential at or below its resting value; it is widely used as a neuronal "silencer" (Johns et al., 1999). Some single amino acid substitutions in the P-loop signature sequence of the channel (Heginbotham et al., 1994), such as G146S (here called Kir2.1-nc), block ion flow without affecting the protein's localization (Haruna et al., 2007). We generated *Drosophila* codon-optimized *UAS-EGFP::Kir2.1* and *UAS-EGFP::Kir2.1-nc* lines and crossed them to the *GH146-GAL4* driver, which directs transgene expression to PNs (Stocker et al., 1997). Whereas the non-conducting Kir2.1-nc variant proved innocuous, the expression of functional Kir2.1 under *GH146-GAL4* control caused early larval lethality, but this premature death could be circumvented with three tubulin promoter-driven copies of the temperature-sensitive repressor of GAL4, $GAL80^{ts}$ (McGuire et al., 2003), which kept the expression of the channel at bay until the block was thermally relieved during adulthood.

Following their induction for 24 h at 31°C, both EGFP-tagged channels (Kir2.1 and Kir2.1-nc) were detected in PNs of 5 day-old adults at comparable levels and in the same anatomical distribution (Fig. 3*A*). Whole-cell current-clamp recordings showed that EGFP::Kir2.1 lowers the input resistance and membrane time constant relative to EGFP::Kir2.1-nc (Fig. 3*B–D*) and powerfully opposes depolarization: Kir2.1-expressing neurons required approximately two-fold larger depolarizing currents to drive spiking across a firing rate range of 1–50 Hz (Fig.

3*E*). Although Kir2.1 does not strictly silence the population of neurons in which it is expressed (the added potassium conductance can always be compensated by a large enough current injection; Figs. 3*B*,*E*), the currents necessary to do so seem difficult to attain *in vivo*.

A simple behavioral test supported this conclusion. Adult-onset expression of Kir2.1 in the PDF-expressing ventral subset of lateral pacemaker neurons (using the *pdf-GAL4* driver) disrupted the circadian locomotor rhythm in constant darkness, as expected (Nitabach et al., 2002), whereas flies expressing Kir2.1-nc remained rhythmic (Fig. 3*F*).

Trans-synaptic regulation of gene expression: transmitter release and synapse remodeling, and a late shift to proteostasis and neuroprotection

To delineate changes in presynaptic gene expression after muting postsynaptic neural activity, we compared the third antennal segment transcriptomes of flies expressing either Kir2.1 or Kir2.1-nc in PNs (Fig. 4*A*). We studied three induction times—12 hours, 48 hours, and 96 hours—in individuals that were age-matched at the point of analysis: all tissues were harvested between ZT6 and ZT7 on the fifth post-eclosion day (Fig. 4*A*). Two sequencing technologies—3' DGE for the 12- and 48-hour groups and standard RNA-seq for the 96-hour group—gave similar mapping metrics (Tables 3 and 4).

For 12-hour induction, experimental (Kir2.1) and control (Kir2.1-nc) flies were placed at 31°C from ZT18 until ZT6 on their fifth post-eclosion day and decapitated between ZT6 and ZT7 on the same day (Fig. 4*A*). Three biological replicates were sequenced for each genotype, one from males and two from females, and sex differences were accounted for and removed by the regression model entered into DESeq2. This analysis highlighted 25 differentially expressed antennal segment genes with FDR-adjusted $p < 0.20$ (Table 5). The average

changes in absolute expression levels of the top 20 differentially expressed genes were about 15-fold smaller than those of the top 20 clock-controlled genes ($\log_2$ fold changes: 0.35 ± 0.08 for homeostatic genes vs.1.9 ± 0.9 for circadian genes; Tables 2 and 5), resulting in many fewer significant hits for the same FDR threshold. Among genes with the smallest FDR-adjusted *p*-values, many are involved in cell fate commitment and morphogenesis (Table 5); eight (*bazooka*, *sugar-free frosting*, *plum*, *prospero*, *Ankyrin 2*, *spätzle*, *Syncrip*, and *ATP6AP2*) have been linked to synaptic organization or synapse formation, however indirectly (Doe et al., 1991; Ruiz-Canada et al., 2004; Koch et al., 2008; Pielage et al., 2008; Baas et al., 2011; Sutcliffe et al., 2013; Yu et al., 2013; Halstead et al., 2014; Dubos et al., 2015).

For 48-hour induction, experimental and control groups were shifted to 31°C at ZT6 of their third post-eclosion day and decapitated between ZT6 and ZT7 on day 5 (Fig. 4*A*). Three biological replicates—all from males—were sequenced for each genotype using 3' DGE technology. One of the Kir2.1-nc replicates did not cluster well with the others (Table 3) and was excluded from the differential expression analysis, which produced 26 hits with FDR-adjusted $p < 0.20$ (Table 6). Conspicuous among these hits were several ribosomal components and three chaperones of the Hsp20 family (Hsp27, Hsp67Bc, and Hsp23) (Haslbeck et al., 2019). At first glance, the upregulation of heat shock proteins might suggest a direct effect of our method of transgene induction (31°C heat), but upon reflection heat cannot explain the observed differences because experimental and control flies were exposed to the same temperature regime. A more plausible explanation is, therefore, that prolonged postsynaptic silencing places an intense homeostatic burden on presynaptic partners which elicits a generalized increase in protein synthesis.

For 96-hour induction, experimental and control groups were kept at 31°C from ZT6 of their first post-eclosion day and again decapitated between ZT6 and ZT7 on day 5 (Fig. 4*A*). A total of 20 libraries were sequenced in two batches using RNA-seq technology. A different sequencing method was chosen to ensure that our results were valid across sequencing platforms, and more replicates were processed to increase sensitivity. The first batch consisted of 12 samples with six replicates from each of the two genotypes (all male third antennal segments). Two replicates of each genotype in the first batch (K96-2, K96-3, C96-2, and C96-3) were sequenced to twice the depth of the others to detect very lowly expressed genes more reliably. The second batch (eight samples in total) consisted of another four samples of each genotype, two each from females and two from males. Two samples (K96-1 and K96-9) had low within-batch correlations and were omitted from the analysis (Table 4). The increase in statistical power enabled the detection of 32 differentially expressed genes with FDR-adjusted $p < 0.05$ after controlling for sex and batch in DESeq2 (Table 7). Three biological processes stand out among these differentially expressed genes. First, six genes related to the Imd and Toll pathways of the innate immune response (Valanne et al., 2011) were strongly downregulated: the pattern recognition receptor PGRP-SD; the antibacterial peptide Drosocin (Dro); the negative regulator of Imd, pirk; and the antimicrobial peptides Bomanin Short 1, 3, and 5 (a.k.a. IM1, IM2, and IM3). Second, chaperones of the Hsp20 family, already encountered after 48-h induction, were again upregulated (Hsp26, Hsp23, and Hsp67Bc) (Haslbeck et al., 2019). And third, four genes involved in programmed cell death were differentially expressed, with two pro-apoptotic factors downregulated—matrix metalloproteinase 1 (Mmp 1) and apoptosis-inducing factor (AIF)—and two gene products inhibiting apoptosis up-regulated (Hsp26, Buffy) (Quinn et al., 2003; Wang et al., 2004; Joza et al., 2008). Overall, the 96-hour picture suggests a transcriptional landscape tilted toward cell protection and maintenance.

To obtain an aerial overview of transcriptionally regulated biological processes during all induction periods, we probed for coordinated changes in functionally related sets of genes via gene ontology (GO) enrichment analyses. These analyses were performed on all differentially expressed genes with unadjusted $p < 0.05$ and included only GO terms with more than 40 attached genes; the enriched GO terms (Fisher's exact test, $p < 0.01$) were then hierarchically clustered according to their semantic similarity (Wang et al., 2007; Brionne et al., 2019) (Fig. 4*B*). After 12 hours of induction, presynaptic transcriptional changes centered on genes encoding synaptic release and remodeling machinery; at 48 hours and beyond, protein synthesis and degradation, and energy metabolism, predominated (Fig. 4*B*,*C*, Tables 8–10). Closer scrutiny of the 81 genes responsible for the early enrichment of synaptic GO annotations (Fig. 4*C*, Tables 11 and 12) uncovered many with established roles in homeostatic plasticity at the NMJ (or with known interactions with such genes), as we discuss below. Although typical transcripts showed only modest expression level changes of 15–30%, their regulation was clearly visible across multiple libraries (Fig. 4*D*). This consistency across biological replicates, and the statistically verified overabundance of synaptic genes in the differentially expressed set with low unadjusted *p*-values (Tables 11 and 12), suggest a genuine signal.

Cross-validation of regulated genes with 3' DGE, RNA-seq, and RT-qPCR

As a further validation of our gene expression measurements, we compared transcriptome-wide 3' DGE with transcriptome-wide RNA-seq data. There was an approximately linear relationship between the average expression levels of all genes in all samples (Fig. 5*A*), with a small departure in lowly expressed genes caused by the extra amplification step in the RNA-seq protocol (see Methods); as a result RNA-seq reported systematically higher expression

384 levels for scarce transcripts than did 3' DGE. For genes transcribed at moderate to high
385 expression levels, the two sequencing platforms were in close agreement.
386
387 We next selected 11 transcripts for RT-qPCR verification. These transcripts were chosen from
388 the set of differentially expressed genes (unadjusted $p < 0.05$; both up- and down-regulated)
389 in the 96-hour induction group and used to validate all deep sequencing data. The fold
390 changes of the 11 chosen transcripts, as estimated by RT-qPCR with normalization to the
391 housekeeping gene *CycK*, correlated tightly with 3' DGE and RNA-seq measurements (Fig.
392 5*B*). This agreement between three independent measures of gene expression, at a
393 transcriptome-wide scale and across several individual genes, lends confidence to our
394 analysis.

Discussion

Trans-synaptic regulation of gene expression

Our study introduces an experimental system for detecting changes in gene expression in response to changes in the electrical excitability of a partner cell. The product of the *Kir2.1* transgene powerfully suppresses the activity of neurons in which it is expressed, while a control transgene, which codes for a potassium channel with a single amino acid substitution in its selectivity filter (Kir2.1-nc), has no effect (Fig. 3*B*–*F*). Isogenic strains expressing one or the other of these transgenes from the same chromosomal locus offer an ideal platform for differential gene expression analyses because differences between them can be pinned to a single codon change in the genome. The finding that prolonged postsynaptic silencing induces the expression of Hsp20 proteins in a manner unrelated to heat shock (Tables 6 and 7) underscores the power of this carefully controlled system.

The same finding, however, also highlights a limitation particular to our current approach. We imposed the Kir2.1 clamp on the first synaptic relay in the *Drosophila* olfactory system because its pre- and postsynaptic elements are easily separable by purely physical means, but this convenience exacted a price: the third antennal segment contains not only ORNs but also glial and support cells, which account for about two thirds of the segment's cell population (Vosshall et al., 1999). We are therefore unable to determine whether the expression of Hsp20 proteins is exclusively or even partially neuronal. Although the same reservation does not apply to the many synaptic genes that are differentially expressed during the early phase of the homeostatic response (Fig. 4*B*,*C*), the presence of non-neuronal contaminants may nevertheless have hindered the detection of low-abundance neuronal transcripts or underestimated their fold change. Both of these drawbacks could be overcome by FACS-

isolation of a genetically labeled cell population before RNA extraction, as would be required as a matter of course in all instances where the synaptic partners are anatomically intermingled. With this extra step, our system will be easily adapted for analyses of transcriptional changes elicited in presynaptic cells by a loss of postsynaptic responsivity, in postsynaptic cells by a loss of presynaptic input, or in glial cells by a heightened demand for synaptic remodeling.

Despite these caveats, many of the early expression level changes we detect affect genes encoding synaptic proteins with known, suspected, or at least plausible roles in homeostatic plasticity (Fig. 4*B*,*C*, Tables 5, 11, and 12) (Davis and Müller, 2015): elements of the wingless signaling system (e.g., Wnk, sgg), which acts as an endogenous suppressor of homeostatic compensation at the NMJ (Marie et al., 2010); the v-SNARE synaptobrevin (nSyb) and its chaperone Nsf2 (Söllner et al., 1993; Bacci et al., 2001); rab3 guanine nucleotide exchange factor (rab3-GEF), which controls the assembly and distribution of active zone components (Bae et al., 2016) and regulates the nucleotide state-dependent association of rab3 with synaptic vesicles, which in turn determines the calcium sensitivity of their release (Geppert et al., 1997; Müller et al., 2011); an active zone resident (unc-13-4a) known to associate with the Rab3-interacting molecule RIM and other active zone components (Schoch et al., 2002; Liu et al., 2011; Müller et al., 2012); a kinesin motor heavy chain (Khc-73) implicated in active zone assembly and synaptic homeostasis (Tsurudome et al., 2010); an active zone-integral guanylate kinase (CASK) that serves as a phosphorylation target of CDK5 (Samuels et al., 2007), which homeostatically regulates presynaptic calcium influx and release probability (Seeburg et al., 2008; Kim and Ryan, 2010); the E3 ubiquitin-protein ligase highwire (hiw) and the Smad protein Medea (Med), which in motor neuron terminals are part of the transduction cascade for a retrograde signal from muscle (Haghighi et

al., 2003; McCabe et al., 2004; Goold and Davis, 2007); the cytoskeletal anchor Ankyrin 2 (Koch et al., 2008; Pielage et al., 2008); and subunits or accessory proteins of voltage-gated ion channels (quiver, ether-á-go-go, Hyperkinetic, paralytic) (Tables 5, 11, and 12). Collectively, these changes could signal an increase in the number of release sites or an expansion of the release-ready vesicle pool, inferred to represent the dominant quantal parameter change during homeostatic matching at ORN-to-PN synapses (Kazama and Wilson, 2008) and one of two homeostatic levers at the NMJ (the other being modulation of calcium influx into the terminal) (Müller et al., 2012).

When drawing comparisons with earlier work, however, it is important to bear in mind experimental differences in the speed of induction and expression of the homeostatic response. Abrupt adult-onset PN silencing resembles an acute postsynaptic receptor blockade at the NMJ more closely than it does the slow developmental processes studied in analyses of arbor size matching in the antennal lobe (Kazama and Wilson, 2008; Mosca and Luo, 2014), but homeostatic compensation at the NMJ is evident within minutes, long before changes in gene expression can occur (Frank et al., 2006). That elements of the homeostatic machinery are encoded by trans-synaptically regulated genes must therefore reflect a secondary layer of feedback control or a more profound reallocation of ORN synapses between PNs and other postsynaptic partners, such as local neurons of the antennal lobe (Groschner and Miesenböck, 2019).

Because changes in the expression levels of putative homeostatic genes are small compared to those of circadian-regulated genes (Figs. 1*D*, 4*C*) , we were forced to apply lenient FDR thresholds to the 12-hour and 48-hour induction experiments, raising the specter of false positives in these data sets. Two observations should allay this concern. First, the 96-hour

induction experiment, whose greater statistical power made the application of a more stringent significance threshold possible, recovered many of the same biological processes and indeed the same genes (e.g., Hsp23, Hsp67Bc) as the statistically weaker 48-hour induction experiment (Tables 9 and 10). Second, our RT-qPCR validation included several genes that failed to cross the most stringent FDR threshold (Fig. 5*B*). These RT-qPCR spot checks confirmed that expression level changes detected by RNA-seq or 3' DGE were accurate. Nonetheless, new candidates emerging from our screen will need to survive rigorous functional studies before joining the ranks of established homeostatic plasticity genes.

Labeling connections with trans-synaptically regulated genes?

Transcriptional changes that are controlled by trans-synaptic signals could be exploited for the generation of new circuit-breaking tools. In most neurobiological studies, the object of interest is not a population of genetically homogeneous neurons but an operational unit—a circuit—defined by connectivity rather than a common genetic marker (Miesenböck and Kevrekidis, 2005). Circuit analyses have benefited greatly from the development of trans-synaptic vectors (Card et al., 1990; Kuypers and Ugolini, 1990; Strack and Loewy, 1990; Wickersham et al., 2007), which travel along synaptic connections between specific types of neuron and serve as vehicles for the distribution of other encodable tools (Sjulson et al., 2016).

Ideally, trans-synaptic expression systems possess a mechanism that allows their initialization at a specific location, a rule that governs their propagation in the network, and gain. Viruses have some of these characteristics (Card et al., 1990; Kuypers and Ugolini, 1990; Strack and Loewy, 1990; Wickersham et al., 2007). Their infectious spread can follow routes of synaptic transmission, and replicative gain (where permitted) allows each infected neuron to supply

more viral particles to its outputs than it receives from its inputs. Viral infections are, however, difficult to control and initialize with single-cell resolution and can produce considerable toxicity and extrasynaptic spread.

Lectins and catalytically crippled neurotoxins are also ferried across synapses (Schwab et al., 1979; Gerfen et al., 1982; Ruda and Coulter, 1982). These stripped-down trans-synaptic tracers lack the cytotoxic effects of viral replication but also the associated gain and the capacity to serve as gene delivery vehicles. The need to carry the label as payload across the synaptic cleft requires high expression levels, which jeopardize the specificity of transfer. Clearly, the ideal trans-synaptic vector would, instead of carrying its own genetic material or marker, act on expression cassettes that lie dormant in the genome of the host organism until switched on by a trans-synaptic signal.

Circuit-tracing systems such as *trans*-Tango, TRACT, and BAcTrace are built on this principle but require the reconstitution of an exogenous, contact- or ligand-based, cell-to-cell signaling apparatus (Huang et al., 2017; Talay et al., 2017; Cachero et al., 2020). This introduces additional genetic complexity and the danger of overexpression artefacts if the foreign molecules escape synaptic confinement. Eavesdropping on endogenous trans-synaptic communication during homeostatic plasticity offers a possible cure for these problems. Imagine a sudden, targeted loss of excitability in a small group of neurons or even a single cell, brought about by the inducible expression of Kir2.1. If presynaptic partners sense this perturbation and compensate homeostatically, the upregulation of plasticity genes could be coupled to the expression of sensors, actuators, transcription factors, or recombinases (Sjulson et al., 2016).

The chief obstacle to the development of this retrograde tracing technology is the small, at most two-fold, changes in homeostatic gene expression we detect (Tables 5, 11, and 12). We suspect that these changes would need to be amplified with adequate signal-to-noise ratio, perhaps by flipping a permanent recombination switch (Sjulson et al., 2016), to be practically useful. Region- or cell-specific differences in the capacity or mechanisms of homeostatic compensation are another potential concern. For example, it is likely that different plasticity mechanisms operate at excitatory and inhibitory synapses (or that the same genes respond to activity perturbations in opposite directions) (Turrigiano, 2011), leaving our hypothetical tracing tool blind to—or, depending on perspective, selective for—one or the other class of input. Still, the substantial overlap between components of the homeostatic machinery at the NMJ (Davis and Müller, 2015) and homeostatically regulated genes in the antennal lobe (Fig. 4*C*) suggests at least a measure of functional conservation from peripheral to central synapses. And, the activity-dependent changes in the expression levels of immediate early genes, which are widely used to capture task-specific neural ensembles (Morgan and Curran, 1991; Sjulson et al., 2016; DeNardo and Luo, 2017), are roughly equal to those of the trans-synaptically regulated genes we have identified.

Author contributions

E.R.H. and G.M. designed the study, analyzed and interpreted the results, and wrote the paper. E.R.H. performed all experiments with the exception of electrophysiological recordings, which were done by D.P.

Figures and Figure Legends

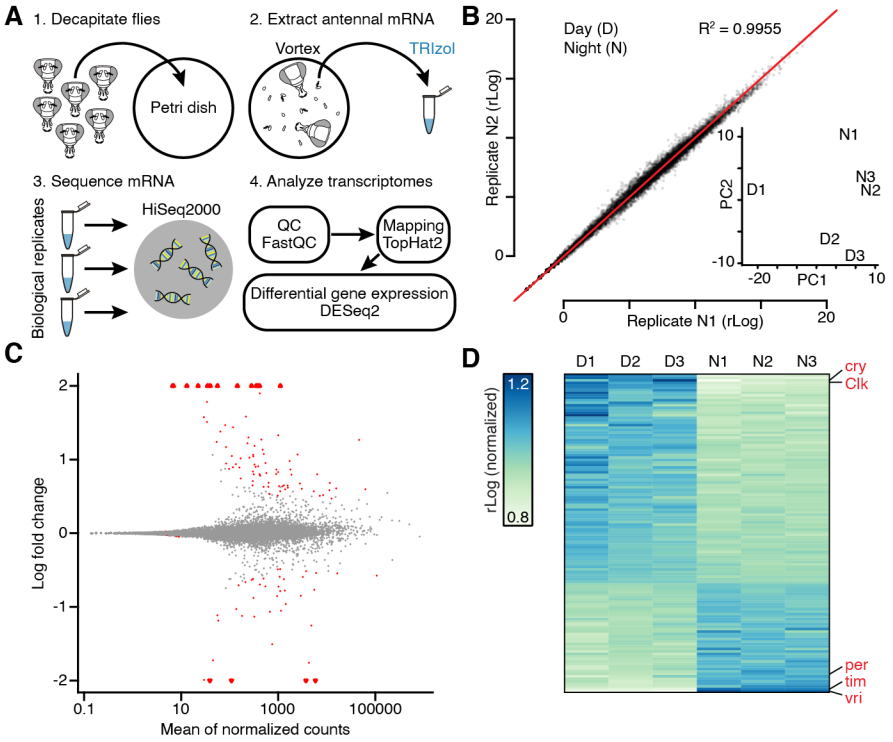

Figure 1. Antennal transcriptomics: workflow, diagnostics, and functional validation. ***A***, Experimental workflow. ***B***, Scatterplot of gene expression levels in biological replicates N1 vs. N2. Inset: D and N samples in a principal component analysis (PCA) plot. ***C***, MA plot of $\log_2$ fold change in expression vs. mean expression level of all transcripts. Triangles represent data points outside the plotted range. ***D***, Expression levels of all transcripts with FDR-adjusted $p < 0.20$ during the day and night. Each column represents a sequencing library generated from third antennal segments. Core clock components are indicated in red.

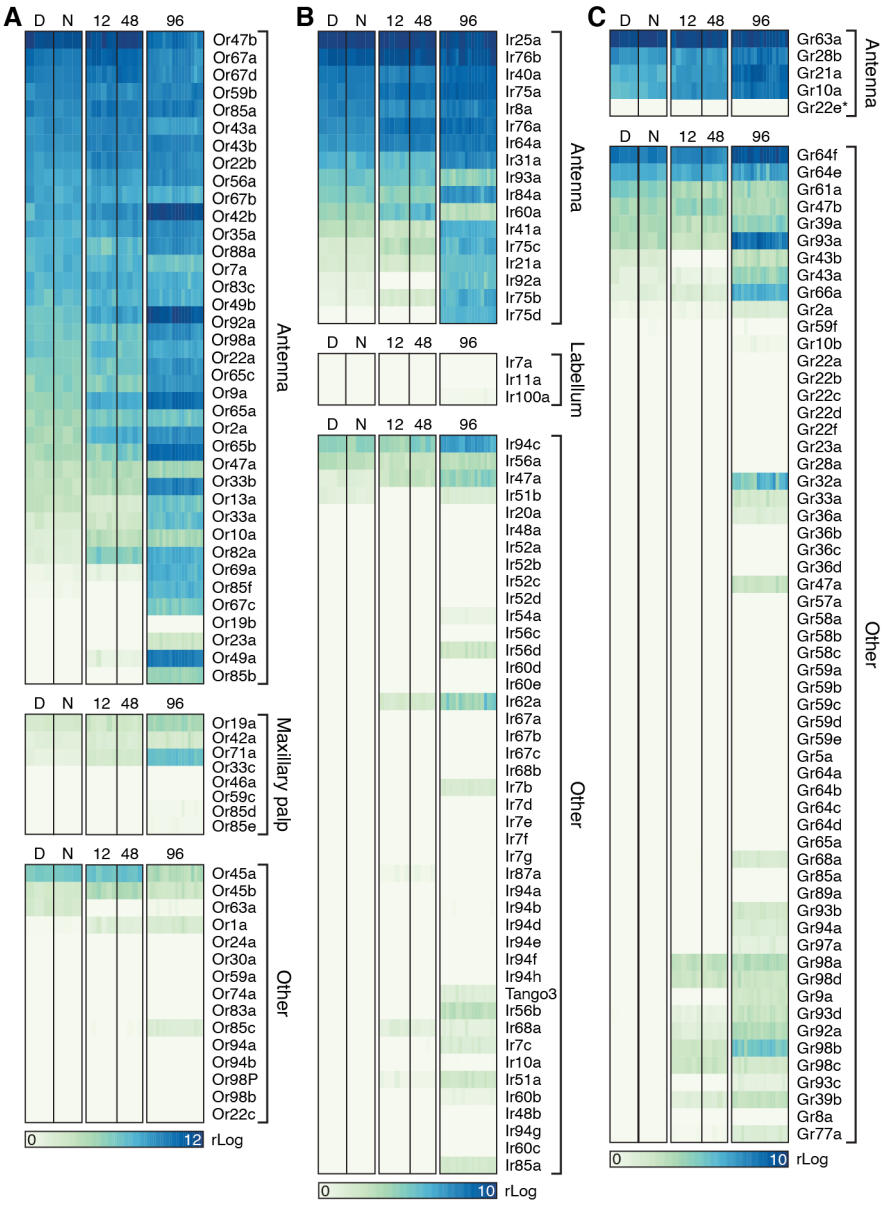

552

553

554 **Figure 2.** Expression levels of ORs (***A***), IRs (***B***), and GRs (***C***) in sequencing libraries

555 generated from third antennal segments. Each column represents a library generated during

556 the day (D) or night (N), or after 12-hour, 48-hour, or 96-hour induction of Kir2.1 or Kir2.1-

557 nc. The gene encoding the obligatory OR coreceptor Orco/Or83b was expressed at a level

558 above those of other *OR* genes (mean rLog ± SEM = 13.6178 ± 0.16503) and omitted from ***A***.

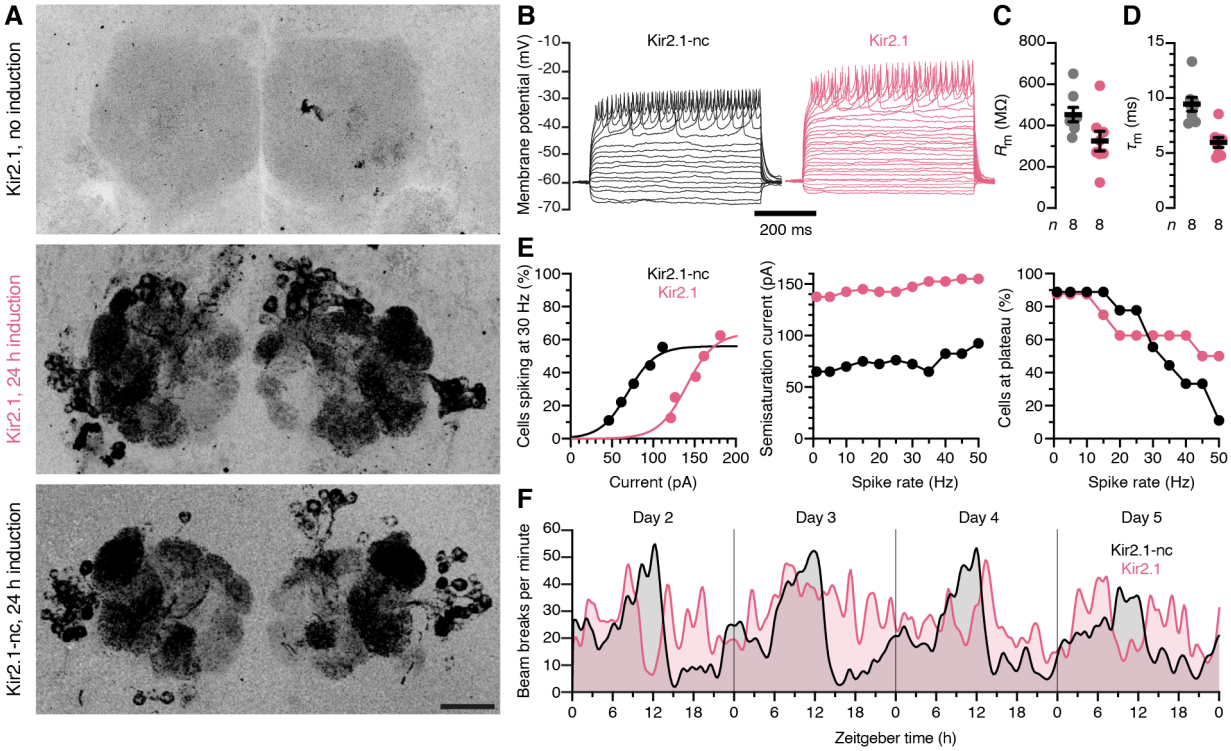

559

560

561 **Figure 3.** A transcriptomics-friendly neuronal activity clamp. ***A***, Maximum intensity
562 projections of confocal image stacks through the antennal lobes of 5-day old female flies
563 carrying *EGFP::Kir2.1* or *EGFP::Kir2.1-nc* transgenes under *GH146-GAL4* and *tub-GAL80^{ts}*
564 control. The expression of Kir2.1 constructs is undetectable at 21˚C (top) but induced at 31˚C
565 (center and bottom). Scale bar, 20 µm. ***B***, Example voltage responses to 5-pA current steps of
566 antennal lobe PNs expressing EGFP::Kir2.1-nc (black) or EGFP::Kir2.1 (red). ***C***, ***D***, Kir2.1
567 (red) lowers the input resistance R_m ($p = 0.0481$, *t*-test; ***C***) and shortens the membrane time
568 constant τ_m ($p = 0.0005$, *t*-test; ***D***) relative to Kir2.1-nc (black). Circles, individual PNs; bars,
569 means ± SEM. ***E***, Cumulative distribution functions of the percentages of PNs reaching a
570 spike frequency of 30 Hz at different levels of injected current (left); semisaturation currents
571 (center) and percentages of cells reaching spike rates of 1–50 Hz, for PNs expressing Kir2.1-
572 nc (black) or Kir2.1 (red). ***F***, Circadian locomotor rhythms in constant darkness. Locomotion
573 was quantified as the total number of midline crossings per minute in groups of 16 flies
574 expressing Kir2.1-nc (black) or Kir2.1 (red) under *pdf-GAL4* control. The traces were

575 smoothed with a Gaussian kernel (1.25 hours FWHM) and show data collected on days 2–5

576 after the flies were transferred to activity monitors.

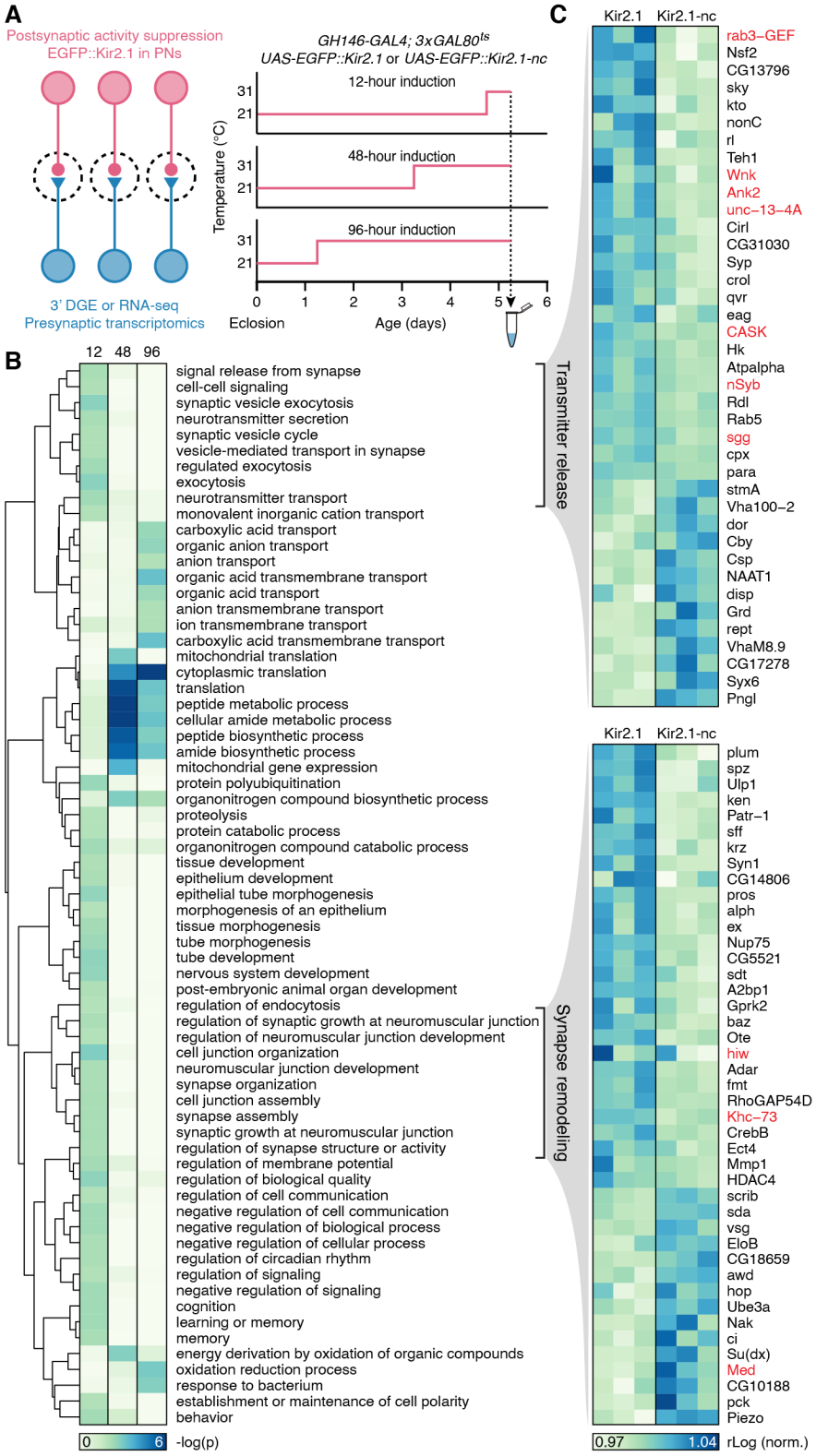

Figure 4. Trans-synaptic regulation of gene expression: transmitter release and synapse remodeling, and a late shift to proteostasis and neuroprotection. ***A***, Experimental design. **B.**

581 Enrichment of GO biological process terms in third antennal segment transcriptomes after 12-
582 hour, 48-hour, and 96-hour induction of Kir2.1. The dendrogram represents semantic
583 groupings among GO terms. ***C***, Expression levels of transcripts attached to two semantic
584 groupings, "transmitter release" and "synapse remodeling" (***B***), after 12 hours of induction of
585 Kir2.1 or Kir2.1-nc. Each column represents a sequencing library. Gene products previously
586 implicated in homeostatic synaptic plasticity (see Discussion) are indicated in red.

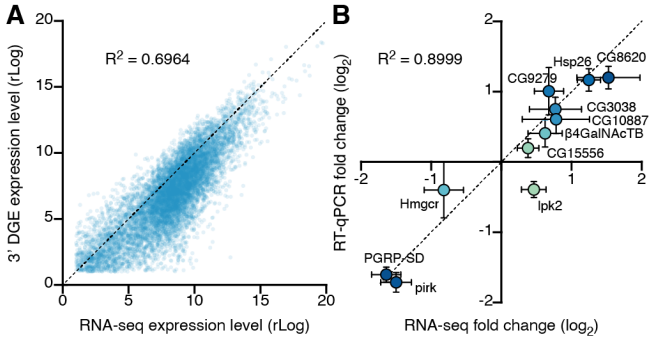

587

588

589 **Figure 5.** Cross-validation of differential gene expression. ***A***, Scatterplot of average gene

590 expression levels determined by RNA-seq vs. 3' DGE. ***B***, Scatterplot of log2 fold changes

591 (means ± SEM) in the expression levels of 11 transcripts after 96-hour induction of Kir2.1,

592 determined by RNA-seq or RT-qPCR.

Tables

Table 1. Mapping metrics of third antennal segment transcriptomes collected during the day (D) and night (N)

ID	*n* Reads	*n* Mapped	% Mapped	*n* Unique	% Unique	Average R^2
D1	20,857,542	14,732,179	70.63%	13,342,850	63.97%	0.9897
D2	19,466,527	14,408,098	74.01%	13,373,355	68.70%	0.9931
D3	18,908,595	14,656,324	77.51%	13,440,037	71.08%	0.9919
N1	22,905,480	18,406,329	80.36%	17,187,773	75.04%	0.9955
N2	21,095,058	16,864,414	79.94%	15,564,220	73.78%	0.9963
N3	23,547,296	18,429,070	78.26%	16,918,247	71.85%	0.9963
Average	21,130,083	16,249,402	76.79%	14,971,080	70.74%	0.9938

Absolute number and percentages of reads aligned to the transcript file of the Berkeley Drosophila Genome Project (BDGP) release 5.74. *n* Reads: number of raw reads; *n* Mapped and % Mapped: number of reads mapping to the reference transcriptome with corresponding percentage; *n* Unique and % Unique: number of reads mapping to a unique location in the reference transcriptome with corresponding percentage; Average R^2: average replicate correlation (Pearson's correlation coefficient calculated across all genes with a non-zero read count in at least one replicate).

605 **Table 2. Circadian-regulated genes (FDR-adjusted $p < 0.01$)**

Gene	Baseline expression	Log_2 fold change	*p*	FDR	Description
vri	3724.50	-4.6985	4.29E-106	3.89E-102	core circadian clock
tim	5834.10	-3.7979	4.29E-78	1.95E-74	core circadian clock
GstD3	1104.77	2.5973	3.46E-28	1.05E-24	glutathione metabolism
CG2016	281.15	2.9593	1.22E-22	2.77E-19	hormone binding
CG33757	410.74	2.9298	1.03E-19	1.87E-16	no functional information
Cyp4d21	4279.26	-1.8094	7.21E-18	1.09E-14	oxidation-reduction process
Clk	143.92	2.9383	2.18E-16	2.82E-13	core circadian clock
CG10026	352.82	2.3039	3.80E-15	4.31E-12	lipid binding
Ugt35b	46348.94	1.3358	3.54E-11	3.56E-08	UDP glycosyl transferase
GstE9	1001.76	1.4003	2.71E-10	2.46E-07	glutathione metabolism
CG31324	749.19	-1.6055	4.71E-09	3.88E-06	no functional information
Pdh	55.97	2.9461	7.75E-09	5.85E-06	receptor dehydrogenase
CG6834	2496.64	1.1409	1.30E-08	9.04E-06	no functional information
CG7208	108.72	-2.2001	1.99E-08	1.29E-05	no functional information
mt:lrRNA	418.18	2.0580	1.64E-07	9.93E-05	mitochondrial translation
CG15096	1139.97	-1.1414	2.08E-07	1.14E-04	transmembrane anion transport
slik	449.97	1.3790	2.14E-07	1.14E-04	cell proliferation
CG9815	39.03	-3.1059	2.43E-07	1.23E-04	no functional information
cu	674.29	-1.1606	3.45E-07	1.57E-04	NADP metabolism
zormin	503.40	1.1680	3.29E-07	1.57E-04	cytoskeletal structure
CG10513	326.16	1.2906	3.72E-07	1.61E-04	no functional information
Ugt86De	477.43	1.2370	5.25E-07	2.17E-04	UDP glycosyl transferase
CG6484	322.18	-1.2398	7.35E-07	2.90E-04	glucose import
CheB93b	215.37	1.7419	1.21E-06	4.56E-04	pheromone detection
CG7149	1784.54	0.9488	1.49E-06	5.42E-04	phosphotransferase
CG31100	1430.28	-1.0624	2.34E-06	8.16E-04	glucose import
CG10433	1716.02	1.0842	2.70E-06	9.06E-04	female receptivity to mating
CG2930	545.58	1.0604	4.77E-06	1.55E-03	transmembrane transport
CG6356	4808.16	-1.4003	5.51E-06	1.72E-03	transmembrane transport
CG33946	117.51	1.6102	5.89E-06	1.78E-03	no functional information
wbl	231.65	1.3672	6.67E-06	1.95E-03	protein folding in ER
CG3625	6333.94	0.8930	7.49E-06	2.12E-03	no functional information
CG31321	34.98	2.6316	8.08E-06	2.22E-03	transmembrane transport
CG13841	243.03	1.4691	1.28E-05	3.42E-03	no functional information
CG7724	912.70	0.9733	1.44E-05	3.74E-03	oxidation-reduction process
Ugt35a	303.93	1.2040	1.63E-05	4.10E-03	UDP glycosyl transferase
CG1698	22.34	3.7173	1.72E-05	4.22E-03	neurotransmitter transport
CG11951	39.60	2.5616	1.79E-05	4.26E-03	proteolysis
mt:ND2	385.70	1.0282	1.84E-05	4.29E-03	mitochondrial electron transport
CG6910	255.13	1.1671	2.27E-05	5.16E-03	oxidation-reduction process
cwo	1095.79	-0.8935	2.82E-05	6.24E-03	circadian regulation of gene expression

606

607 *p*, unadjusted *p*-value; FDR, *p*-value adjusted for multiple comparisons.

Table 3. Mapping metrics for third antennal segment transcriptomes collected after 12 or 48 hours of induction of Kir2.1 (K) or a non-conducting control (C)

ID	*n* Reads	*n* Mapped	% Mapped	*n* Unique	% Unique	Average R^2
K12-1	29,660,291	15,855,218	53.46%	14,082,433	47.48%	0.9939
K12-2	28,904,100	15,808,260	54.69%	14,110,730	48.82%	0.9943
K12-3	28,938,152	15,549,498	53.73%	13,323,889	46.04%	0.9935
C12-1	22,023,606	10,963,417	49.78%	9,701,601	44.05%	0.9941
C12-2	15,850,790	8,864,492	55.93%	7,922,966	49.99%	0.9947
C12-3	11,834,929	6,237,128	52.70%	5,546,857	46.87%	0.9946
K48-1	28,004,316	18,815,975	67.19%	16,487,747	58.88%	0.9953
K48-2	17,661,910	11,229,908	63.58%	9,851,297	55.78%	0.9951
K48-3	27,158,740	15,643,356	57.60%	13,588,111	50.03%	0.9957
C48-1	40,636,120	26,365,750	64.88%	23,831,661	58.65%	0.9770
C48-2	26,993,657	13,344,752	49.44%	11,474,648	42.51%	0.9612
C48-3	32,525,963	18,944,019	58.24%	17,227,196	52.96%	0.9787
Average	**25,849,381**	**14,801,814**	**56.77%**	**13,095,761**	**50.17%**	**0.9890**

Absolute number and percentages of reads aligned to the transcript file of the Berkeley Drosophila Genome Project (BDGP) release 5.74. *n* Reads: number of raw reads; *n* Mapped and % Mapped: number of reads mapping to the reference transcriptome with corresponding percentage; *n* Unique and % Unique: number of reads mapping to a unique location in the reference transcriptome with corresponding percentage; Average R^2: average replicate correlation (Pearson's correlation coefficient calculated across all genes with a non-zero read count in at least one replicate).

Table 4. Mapping metrics for third antennal segment transcriptomes collected after 96 hours of induction of Kir2.1 (K) or a non-conducting control (C)

ID	*n* Reads	*n* Mapped	% Mapped	*n* Unique	% Unique	Average R^2
K96-1	31,213,542	25,030,748	80.19%	14,405,148	46.15%	0.9836
K96-2	55,190,242	43,522,921	78.86%	26,736,203	48.44%	0.9937
K96-3	58,556,838	47,205,802	80.62%	31,655,311	54.06%	0.9941
K96-4	29,803,652	24,632,464	82.65%	17,888,586	60.02%	0.9933
K96-5	28,647,909	23,564,548	82.26%	17,152,909	59.87%	0.9937
K96-6	31,030,362	23,420,613	75.48%	17,208,103	55.46%	0.9925
K96-7	26,014,249	21,066,849	80.98%	14,655,033	56.33%	0.9932
K96-8	30,622,108	24,934,568	81.43%	17,368,348	56.72%	0.9928
K96-9	35,563,235	27,845,191	78.30%	14,971,400	42.10%	0.9869
K96-10	26,388,734	21,106,014	79.98%	13,725,816	52.01%	0.9904
C96-1	29,748,012	24,036,358	80.80%	15,070,224	50.66%	0.9928
C96-2	61,127,179	48,487,739	79.32%	30,257,167	49.50%	0.9933
C96-3	58,864,472	49,116,496	83.44%	36,050,234	61.24%	0.9939
C96-4	30,582,966	25,278,565	82.66%	17,865,165	58.42%	0.9928
C96-5	27,223,175	22,593,695	82.99%	16,178,509	59.43%	0.9935
C96-6	29,951,768	24,706,089	82.49%	17,520,016	58.49%	0.9908
C96-7	32,514,120	26,933,883	82.84%	19,342,591	59.49%	0.9940
C96-8	27,902,225	23,365,715	83.74%	17,388,108	62.32%	0.9936
C96-9	28,058,965	21,639,543	77.12%	11,934,889	42.54%	0.9911
C96-10	28,737,234	23,114,269	80.43%	14,720,484	51.22%	0.9928
Average	**35,387,049**	**28,580,104**	**80.83%**	**19,104,712**	**54.22%**	**0.9921**

Absolute number and percentages of reads aligned to the transcript file of the Berkeley Drosophila Genome Project (BDGP) release 5.74. *n* Reads: number of raw reads; *n* Mapped and % Mapped: number of reads mapping to the reference transcriptome with corresponding percentage; *n* Unique and % Unique: number of reads mapping to a unique location in the reference transcriptome with corresponding percentage; Average R^2: average replicate correlation (Pearson's correlation coefficient calculated across all genes with a non-zero read count in at least one replicate).

Table 5. Differentially expressed genes after 12 hours of Kir2.1 induction (FDR-adjusted $p < 0.20$)

Gene	Baseline expression	Log_2 fold change	*p*	FDR	Description
CG11550	7106.49	-0.3861	3.07E-06	4.71E-03	lipid binding
Rbfox1	1799.04	0.3151	3.22E-05	1.35E-02	RNA binding
Trc8	885.38	-0.5493	5.29E-05	1.35E-02	protein ubiquitination
baz	2163.42	0.3019	4.58E-05	1.35E-02	cell polarity, junction formation
Dso1	91551.91	-0.2967	4.77E-05	1.35E-02	immune response
lncRNA:noe	89869.98	0.3187	1.95E-05	1.35E-02	no functional information
GstE3	2132.39	0.3211	2.19E-04	4.80E-02	glutathione metabolism
hth	11449.58	0.2245	3.91E-04	6.65E-02	brain development
sff	1232.13	0.4033	3.58E-04	6.65E-02	NMJ development
plum	981.88	0.4713	4.66E-04	7.14E-02	axon pruning
CG11873	977.85	0.3519	6.28E-04	8.74E-02	stress response, transcription
pros	1847.93	0.3498	9.49E-04	1.21E-01	neuronal differentiation
Ank2	4808.04	0.3167	1.68E-03	1.30E-01	membrane scaffolding
CG6421	1256.69	-0.3262	1.70E-03	1.30E-01	immune response
Hcf	801.97	0.5215	1.44E-03	1.30E-01	chromatic remodeling
Kr-h2	805.79	-0.3513	1.59E-03	1.30E-01	membrane organization
Pis	1370.97	0.2670	1.44E-03	1.30E-01	signal transduction
crol	1882.00	0.2505	1.69E-03	1.30E-01	cell adhesion
sdt	1635.14	0.3144	1.52E-03	1.30E-01	cell polarity, junction formation
spz	755.96	0.4628	1.34E-03	1.30E-01	axon guidance, immune response
Syp	3782.12	0.2909	1.84E-03	1.34E-01	RNA binding, NMJ transmission
ATP6AP2	1413.52	-0.3679	2.08E-03	1.45E-01	axonal transport
CG9171	697.10	0.3263	2.27E-03	1.45E-01	O-linked mannosylation
RpL38	9770.50	-0.2603	2.25E-03	1.45E-01	translation
mAcon1	1385.07	-0.3415	2.80E-03	1.65E-01	mitochondrial Krebs cycle
CG3907	2306.39	-0.2459	2.75E-03	1.65E-01	no functional information

p, unadjusted *p*-value; FDR, *p*-value adjusted for multiple comparisons.

Table 6. Differentially expressed genes after 48 hours of Kir2.1 induction (FDR-adjusted $p < 0.20$)

Gene	Baseline expression	Log_2 fold change	*p*	FDR	Description
CG8620	36.69	2.2870	1.36E-09	1.27E-05	no functional information
CG42502	7610.35	0.7250	7.72E-07	3.60E-03	no functional information
Hsp27	141.78	1.1780	8.78E-06	2.73E-02	HSP20-like chaperone
BomS3	287.22	1.0470	1.41E-05	3.28E-02	immune response
CR41619	337.93	0.9580	1.77E-05	3.30E-02	no functional information
Fbp2	49.24	-1.3890	3.64E-05	5.65E-02	alcohol dehydrogenase
RpLP2	13612.76	0.7030	4.39E-05	5.84E-02	structural constituent of ribosome
Mst57Dc	10.73	-1.5090	5.61E-05	5.91E-02	mating behavior
S-Lap4	8.45	-1.4820	5.71E-05	5.91E-02	proteolysis
CG5986	566.50	1.0110	6.91E-05	6.44E-02	RNA binding
CG3224	171.53	0.9550	8.83E-05	7.48E-02	ribosomal export
CR31032	31.67	1.4380	1.04E-04	8.06E-02	no functional information
Trx-2	4120.04	0.6480	1.12E-04	8.06E-02	thioredoxin, oxidative stress
Cyp4g1	46.34	-1.5000	1.23E-04	8.23E-02	oxidation-reduction
CG7920	1911.26	-0.6730	1.59E-04	8.23E-02	acetyl CoA metabolism
Hsp67Bc	54.45	1.3110	1.51E-04	8.23E-02	translation, protein folding
Jon65Aiv	22.70	-1.4610	1.52E-04	8.23E-02	proteolysis
mRpS5	722.02	0.7000	1.52E-04	8.23E-02	structural constituent of ribosome
RpS3A	31350.61	0.5610	1.81E-04	8.89E-02	structural constituent of ribosome
Tsp39D	1213.20	0.5520	2.08E-04	9.69E-02	cell membrane scaffolding
CG17454	4301.55	0.5740	3.44E-04	1.50E-01	mRNA splicing
CG6770	41760.18	0.4970	3.70E-04	1.50E-01	transcriptional regulation
Pkd2	10.79	1.3760	3.58E-04	1.50E-01	cation transport
Hsp23	141.98	1.0130	4.67E-04	1.81E-01	protein folding
Obp99d	176.07	1.0220	5.51E-04	1.98E-01	smell perception
snRNA:U2:34ABa	106.57	1.3060	5.49E-04	1.98E-01	mRNA splicing

p, unadjusted *p*-value; FDR, *p*-value adjusted for multiple comparisons.

638 **Table 7. Differentially expressed genes after 96 hours of Kir2.1 induction (FDR-adjusted**
639 ***p* < 0.05)**
640

Gene	Baseline expression	Log_2 fold change	*p*	FDR	Description
PGRP-SD	1238.04	-1.6430	3.48E-15	2.70E-11	immune response
Dro	126.09	-2.7530	2.58E-14	1.00E-10	immune response
Hsp26	339.18	1.2540	4.48E-14	1.16E-10	protein folding
pirk	334.11	-1.5010	5.40E-12	1.05E-08	immune response
Obp56a	254.68	-1.1930	9.49E-10	1.48E-06	smell perception
CG10332	160.81	-2.0950	1.48E-09	1.92E-06	no functional information
CG42305	23576.53	1.0490	3.47E-09	3.85E-06	no functional information
Gr32a	76.38	-2.3570	8.22E-09	7.99E-06	smell perception
Hsp23	102.45	1.4180	6.87E-08	5.93E-05	protein folding
ple	2790.60	-0.5390	1.77E-07	1.38E-04	tyrosine hydroxylase
CG42821	879.82	-0.9580	4.02E-07	2.84E-04	no functional information
SiaT	632.96	-0.6810	1.27E-06	8.23E-04	NMJ development
BomS2	73.43	-1.1840	1.73E-06	1.03E-03	immune response
Hsp67Bc	115.73	1.2100	2.45E-06	1.36E-03	translation, protein folding
CG5346	1828.19	-0.5430	3.64E-06	1.89E-03	oxidation/reduction process
Jhe	539.44	-1.6050	8.94E-06	4.35E-03	hormone esterase activity
CG16700	884.33	-0.3650	1.18E-05	5.41E-03	amino acid transporter
CG8303	573.39	-0.7870	1.69E-05	7.29E-03	fatty acyl-CoA metabolism
CG8788	1213.87	0.4020	2.57E-05	9.99E-03	no functional information
Gmap	4141.22	-0.4680	2.44E-05	9.99E-03	vesicle-mediated transport
ZnT63C	451.25	-0.4730	3.00E-05	1.11E-02	Zinc transport
Hnf4	1345.62	-0.3230	4.59E-05	1.62E-02	glucose homeostasis
CG12290	3289.24	-0.3730	5.63E-05	1.90E-02	GPCR, rhodopsin-like
BomS1	912.15	-0.7730	9.49E-05	3.07E-02	immune response
CG18302	11179.04	0.3620	1.02E-04	3.15E-02	lipid metabolism
CG3301	759.35	0.4310	1.09E-04	3.15E-02	steriod dehydrogenase
Mmp1	5100.38	-0.3990	1.07E-04	3.15E-02	cell adhesion
AIF	515.32	-0.4530	1.45E-04	3.93E-02	apoptosis inducing factor
CG15890	1533.66	-0.3050	1.46E-04	3.93E-02	transmembrane transporter
BomS3	413.55	-0.7560	1.52E-04	3.94E-02	immune response
Buffy	355.39	0.4910	1.85E-04	4.64E-02	inhibits programmed cell death
CG34456	604.69	0.5120	2.06E-04	5.00E-02	no functional information

641
642 *p*, unadjusted *p*-value; FDR, *p*-value adjusted for multiple comparisons.

643 **Table 8. Enriched GO biological process terms after 12 hours of Kir2.1 induction**
644

GO id	Term	Annotated	Observed	Expected	Fisher's *p*
GO:0034330	cell junction organization	273	27	14	1.20E-03
GO:0006887	exocytosis	75	11	4	1.80E-03
GO:0016079	synaptic vesicle exocytosis	44	8	2	1.90E-03
GO:0035295	tube development	550	45	29	2.00E-03
GO:0065008	regulation of biological quality	888	66	47	2.20E-03
GO:0060562	epithelial tube morphogenesis	373	33	20	2.40E-03
GO:0007399	nervous system development	843	63	45	2.50E-03
GO:0000209	protein polyubiquitination	58	9	3	3.20E-03
GO:0035239	tube morphogenesis	400	34	21	3.90E-03
GO:0007611	learning or memory	119	14	6	4.00E-03
GO:0050890	cognition	119	14	6	4.00E-03
GO:1901565	organonitrogen compound catabolic process	327	29	17	4.20E-03
GO:0006836	neurotransmitter transport	95	12	5	4.20E-03
GO:0010648	negative regulation of cell communication	241	23	13	4.30E-03
GO:0023057	negative regulation of signaling	241	23	13	4.30E-03
GO:0045055	regulated exocytosis	50	8	3	4.40E-03
GO:0048519	negative regulation of biological process	1047	74	56	4.40E-03
GO:0042391	regulation of membrane potential	51	8	3	5.00E-03
GO:0048729	tissue morphogenesis	483	39	26	5.00E-03
GO:0007610	behavior	377	32	20	5.20E-03
GO:0007269	neurotransmitter secretion	74	10	4	5.40E-03
GO:0099643	signal release from synapse	74	10	4	5.40E-03
GO:0034329	cell junction assembly	176	18	9	5.40E-03
GO:0007613	memory	86	11	5	5.50E-03
GO:0051124	synaptic growth at NMJ	111	13	6	5.70E-03
GO:0007416	synapse assembly	137	15	7	5.80E-03
GO:0007528	neuromuscular junction development	138	15	7	6.20E-03
GO:0060429	epithelium development	730	54	39	6.40E-03
GO:0008582	regulation of synaptic growth at NMJ	88	11	5	6.50E-03
GO:0050808	synapse organization	221	21	12	6.60E-03
GO:0050803	regulation of synapse structure or activity	139	15	7	6.60E-03
GO:0048523	negative regulation of cellular process	914	65	49	6.80E-03
GO:0042752	regulation of circadian rhythm	65	9	3	6.90E-03
GO:0048569	post-embryonic animal organ development	371	31	20	7.40E-03
GO:0007267	cell-cell signaling	326	28	17	7.50E-03
GO:0009888	tissue development	786	57	42	7.70E-03
GO:0099003	vesicle-mediated transport in synapse	78	10	4	7.80E-03
GO:0099504	synaptic vesicle cycle	78	10	4	7.80E-03
GO:0010646	regulation of cell communication	595	45	32	8.70E-03
GO:0023051	regulation of signaling	595	45	32	8.70E-03
GO:0007163	establishment or maintenance of cell polarity	171	17	9	9.00E-03
GO:0015672	monovalent inorganic cation transport	92	11	5	9.10E-03
GO:0030163	protein catabolic process	228	21	12	9.30E-03

GO:0002009	morphogenesis of an epithelium	470	37	25	9.30E-03
GO:0006508	proteolysis	471	37	25	9.60E-03
GO:1904396	regulation of NMJ development	93	11	5	9.80E-03
GO:0030100	regulation of endocytosis	46	7	2	1.00E-02

Annotated, number of genes in the universe attached to a GO term; Observed, number of differentially expressed genes (unadjusted $p < 0.05$) attached to a GO term; Expected, number of genes expected by chance to be attached to a GO term

649 **Table 9. Enriched GO biological process terms after 48 hours of Kir2.1 induction**
650
651

GO id	Term	Annotated	Observed	Expected	Fisher's *p*
GO:0043603	cellular amide metabolic process	405	53	25	8.70E-08
GO:0006518	peptide metabolic process	355	46	22	9.00E-07
GO:0006412	translation	265	37	16	1.90E-06
GO:0043043	peptide biosynthetic process	293	39	18	3.40E-06
GO:0043604	amide biosynthetic process	311	40	19	5.90E-06
GO:0002181	cytoplasmic translation	100	18	6	3.30E-05
GO:0140053	mitochondrial gene expression	86	15	5	2.10E-04
GO:0032543	mitochondrial translation	79	13	5	9.90E-04
GO:1901566	organonitrogen compound biosynthetic process	554	52	34	1.28E-03
GO:0015980	energy derivation by oxidation of organic compounds	54	10	3	1.50E-03

652
653 Annotated, number of genes in the universe attached to a GO term; Observed, number of
654 differentially expressed genes (unadjusted $p < 0.05$) attached to a GO term; Expected, number
655 of genes expected by chance to be attached to a GO term

Table 10. Enriched GO biological process terms after 96 hours of Kir2.1 induction

GO id	Term	Annotated	Observed	Expected	Fisher's *p*
GO:0002181	cytoplasmic translation	100	28	8	5.50E-09
GO:1903825	organic acid transmembrane transport	42	11	4	4.90E-04
GO:1905039	carboxylic acid transmembrane transport	42	11	4	4.90E-04
GO:0043603	cellular amide metabolic process	405	53	34	5.70E-04
GO:0043604	amide biosynthetic process	311	43	26	6.10E-04
GO:0006412	translation	265	38	22	6.30E-04
GO:0006518	peptide metabolic process	355	47	30	9.10E-04
GO:0055114	oxidation-reduction process	308	42	26	9.40E-04
GO:0043043	peptide biosynthetic process	293	40	25	1.22E-03
GO:0009617	response to bacterium	158	25	13	1.32E-03
GO:0015711	organic anion transport	89	16	7	2.59E-03
GO:0046942	carboxylic acid transport	59	12	5	3.03E-03
GO:0015849	organic acid transport	60	12	5	3.51E-03
GO:1901566	organonitrogen compound biosynthetic process	554	63	46	6.21E-03
GO:0034220	ion transmembrane transport	160	23	13	6.94E-03
GO:0098656	anion transmembrane transport	58	11	5	7.74E-03
GO:0006820	anion transport	118	18	10	8.80E-03

Annotated, number of genes in the universe attached to a GO term; Observed, number of differentially expressed genes (unadjusted $p < 0.05$) attached to a GO term; Expected, number of genes expected by chance to be attached to a GO term

Table 11. Differentially expressed genes ($p < 0.05$) attached to GO biological process terms in the semantic grouping "transmitter release" after 12 hours of Kir2.1 induction

Gene	Baseline expression	Log_2 fold change	*p*
Ank2	4808.04	0.3167	1.68E-03
crol	1882.00	0.2505	1.69E-03
Syp	3782.12	0.2909	1.84E-03
ATP6AP2	1413.52	-0.3679	2.08E-03
Pngl	165.57	-0.5711	2.84E-03
Nsf2	57.11	1.0758	4.99E-03
sky	574.22	0.4143	5.49E-03
CG13796	98.20	0.7603	5.64E-03
rab3-GEF	74.57	0.9719	5.81E-03
Atpalpha	25649.53	0.2121	7.80E-03
rept	43.03	-0.9271	1.06E-02
nSyb	7467.28	0.1791	1.25E-02
Cirl	753.00	0.2911	1.37E-02
Teh1	490.53	0.3833	1.47E-02
CG17278	103.00	-0.6499	1.91E-02
Grd	36.96	-0.9307	1.93E-02
Cby	442.89	-0.3202	2.13E-02
Syx6	229.68	-0.4827	2.22E-02
rl	129.67	0.5579	2.28E-02
Vha100-2	1861.65	-0.2887	2.39E-02
eag	1418.20	0.2192	2.62E-02
NAAT1	301.63	-0.3582	2.92E-02
qvr	751.52	0.2494	2.93E-02
Rab5	6457.41	0.1526	3.09E-02
kto	125.71	0.5835	3.33E-02
Csp	246.20	-0.3718	3.50E-02
Rdl	9593.74	0.1719	3.67E-02
para	15702.82	0.1020	3.70E-02
CASK	2105.66	0.1889	3.73E-02
stmA	1105.17	-0.2661	4.04E-02
Hk	1229.40	0.1803	4.22E-02
disp	51.74	-0.7734	4.23E-02
nonC	55.67	0.7504	4.33E-02
unc-13-4A	244.53	0.3676	4.53E-02
Wnk	233.48	0.4181	4.57E-02
cpx	9807.02	0.1367	4.78E-02
sgg	3797.38	0.1451	4.83E-02
CG31030	278.71	0.3348	4.92E-02
dor	43.31	-0.7143	4.99E-02

Table 12. Differentially expressed genes ($p < 0.05$) attached to GO biological process terms in the semantic grouping "synapse remodeling" after 12 hours of Kir2.1 induction

Gene	Baseline expression	Log_2 fold change	*p*
Rbfox1	1799.04	0.3151	3.22E-05
baz	2163.42	0.3019	4.58E-05
sff	1232.13	0.4033	3.58E-04
plum	981.88	0.4713	4.66E-04
Piezo	200.21	-0.6974	6.79E-04
pros	1847.93	0.3498	9.49E-04
spz	755.96	0.4628	1.34E-03
sdt	1635.14	0.3144	1.52E-03
ken	135.28	0.6630	2.10E-03
Su(dx)	557.27	-0.4424	4.47E-03
krz	352.41	0.4352	4.47E-03
awd	1639.43	-0.3123	4.61E-03
Patr-1	38.20	1.0956	6.97E-03
HDAC4	3937.61	0.1914	7.18E-03
alph	1833.82	0.3419	8.46E-03
jus	1553.93	-0.2206	1.04E-02
Khc-73	1436.43	0.2236	1.07E-02
CG14806	119.88	0.6016	1.07E-02
Syn1	224.74	0.4885	1.60E-02
Med	127.02	-0.6286	1.66E-02
pck	104.18	-0.6858	1.71E-02
Ulp1	140.50	0.6389	1.91E-02
Ote	25.41	1.0066	1.92E-02
vsg	1464.00	-0.2474	1.94E-02
hop	663.22	-0.1699	2.02E-02
Nup75	250.20	0.3893	2.12E-02
scrib	1348.95	-0.2035	2.65E-02
Adar	479.31	0.3031	2.78E-02
ci	133.51	-0.5603	2.86E-02
Ect4	958.87	0.2181	2.95E-02
hiw	264.24	0.3638	3.48E-02
RhoGAP54D	9.86	1.1083	3.48E-02
Gprk2	635.86	0.3247	3.50E-02
Ube3a	161.07	-0.4591	3.51E-02
Nak	219.26	-0.4719	3.60E-02
CG10188	43.14	-0.9196	4.28E-02
CG18659	166.96	-0.4214	4.41E-02
fmt	983.41	0.2500	4.52E-02
Mmp1	3792.36	0.2127	4.57E-02
CG5521	26.02	0.9428	4.65E-02
ex	55.44	0.7311	4.73E-02
CrebB	1128.36	0.2159	4.86E-02
EloB	691.48	-0.2662	4.99E-02

670 **References**

671

672 Alexa A, Rahnenführer J, Lengauer T (2006) Improved scoring of functional groups from
673 gene expression data by decorrelating GO graph structure. Bioinformatics, 22:1600–1607.

674

675 Andrews S (2010) FastQC: A quality control tool for high throughput sequence data.
676 https://www.bioinformatics.babraham.ac.uk/projects/fastqc/

677

678 Baas S, Sharrow M, Kotu V, Middleton M, Nguyen K, Flanagan-Steet H, Aoki K, Tiemeyer
679 M (2011) Sugar-free frosting, a homolog of SAD kinase, drives neural-specific glycan
680 expression in the Drosophila embryo. Development, 138:553–563.

681

682 Bacci A, Coco S, Pravettoni E, Schenk U, Armano S, Frassoni C, Verderio C, De Camilli P,
683 Matteoli M (2001) Chronic blockade of glutamate receptors enhances presynaptic release and
684 downregulates the interaction between synaptophysin-synaptobrevin-vesicle-associated
685 membrane protein 2. J Neurosci, 21:6588–6596.

686

687 Bae H, Chen S, Roche JP, Ai M, Wu C, Diantonio A, Graf ER (2016) Rab3-GEF controls
688 active zone development at the Drosophila neuromuscular junction. eNeuro, 3: e0031-
689 16.2016.

690

691 Benton R, Vannice KS, Gomez-Diaz C, Vosshall LB (2009) Variant ionotropic glutamate
692 receptors as chemosensory receptors in Drosophila. Cell, 136:149–162.

693

694 Bolger AM, Lohse M, Usadel B (2014) Trimmomatic: a flexible trimmer for Illumina
695 sequence data. Bioinformatics, 30:2114–2120.
696
697 Brionne A, Juanchich A, Hennequet-Antier C (2019) ViSEAGO: a Bioconductor package for
698 clustering biological functions using Gene Ontology and semantic similarity. BioData Min,
699 12:16.
700 Burrone J, O'Byrne M, Murthy VN (2002) Multiple forms of synaptic plasticity triggered by
701 selective suppression of activity in individual neurons. Nature, 420:414–418.
702
703 Cachero S, Gkantia M, Bates AS, Frechter S, Blackie L, McCarthy A, Sutcliffe B, Strano A,
704 Aso Y, Jefferis GSXE (2020) BAcTrace, a tool for retrograde tracing of neuronal circuits in
705 Drosophila. Nat Methods, https://doi.org/10.1038/s41592-020-00989-1
706
707 Card JP, Rinaman L, Schwaber JS, Miselis RR, Whealy ME, Robbins AK, Enquist LW
708 (1990) Neurotropic properties of pseudorabies virus: uptake and transneuronal passage in the
709 rat central nervous system. J Neurosci, 10:1974–1994.
710
711 Claridge-Chang A, Wijnen H, Naef F, Boothroyd C, Rajewsky N, Young MW (2001)
712 Circadian regulation of gene expression systems in the Drosophila head. Neuron, 32:657–671.
713
714 Clyne PJ, Warr CG, Freeman MR, Lessing D, Kim J, Carlson JR (1999) A novel family of
715 divergent seven-transmembrane proteins: candidate odorant receptors in Drosophila. Neuron,
716 22:327–338.
717

718 Cull-Candy SG, Miledi R, Trautmann A, Uchitel OD (1980) On the release of transmitter at
719 normal, myasthenia gravis and myasthenic syndrome affected human end-plates. J Physiol,
720 299:621–638.
721
722 Davis GW, DiAntonio A, Petersen SA, Goodman CS (1998) Postsynaptic PKA controls
723 quantal size and reveals a retrograde signal that regulates presynaptic transmitter release in
724 Drosophila. Neuron, 20:305–315.
725
726 Davis GW, Müller M (2015) Homeostatic control of presynaptic neurotransmitter release.
727 Annual review of physiology, 77:251–270.
728
729 DeNardo L, Luo L (2017) Genetic strategies to access activated neurons. Curr Opin
730 Neurobiol, 45:121–129.
731
732 Desai NS, Rutherford LC, Turrigiano GG (1999) Plasticity in the intrinsic excitability of
733 cortical pyramidal neurons. Nat Neurosci, 2:515–520.
734
735 Doe CQ, Chu-LaGraff Q, Wright DM, Scott MP (1991) The prospero gene specifies cell fates
736 in the Drosophila central nervous system. Cell, 65:451–464.
737
738 Donlea JM, Pimentel D, Miesenböck G (2014) Neuronal machinery of sleep homeostasis in
739 Drosophila. Neuron, 81:860–872.
740
741 Dubos A, Castells-Nobau A, Meziane H, Oortveld MA, Houbaert X, Iacono G, Martin C,
742 Mittelhaeuser C, Lalanne V, Kramer JM, Bhukel A, Quentin C, Slabbert J, Verstreken P,

743 Sigrist SJ, Messaddeq N, Birling MC, Selloum M, Stunnenberg HG, Humeau Y, Schenck A
744 et al. (2015) Conditional depletion of intellectual disability and Parkinsonism candidate gene
745 ATP6AP2 in fly and mouse induces cognitive impairment and neurodegeneration. Hum Mol
746 Genet, 24:6736–6755.
747
748 Frank CA, Kennedy MJ, Goold CP, Marek KW, Davis GW (2006) Mechanisms underlying
749 the rapid induction and sustained expression of synaptic homeostasis. Neuron, 52:663–677.
750
751 Gao Q, Chess A (1999) Identification of candidate Drosophila olfactory receptors from
752 genomic DNA sequence. Genomics, 60:31–9.
753
754 Geppert M, Goda Y, Stevens CF, Südhof TC (1997) The small GTP-binding protein Rab3A
755 regulates a late step in synaptic vesicle fusion. Nature, 387:810–814.
756
757 Gerfen CR, O'Leary DD, Cowan WM (1982) A note on the transneuronal transport of
758 wheat germ agglutinin-conjugated horseradish peroxidase in the avian and rodent visual
759 systems. Exp Brain Res, 48:443–448.
760
761 Goold CP, Nicoll RA (2010) Single-cell optogenetic excitation drives homeostatic synaptic
762 depression. Neuron, 68:512–528.
763
764 Goold CP, Davis GW (2007) The BMP ligand Gbb gates the expression of synaptic
765 homeostasis independent of synaptic growth control. Neuron, 56:109–123.
766

767 Groschner LN, Miesenböck G (2019) Mechanisms of sensory discrimination: Insights from
768 Drosophila olfaction. Annu Rev Biophys, 48:209–229.
769
770 Haghighi AP, McCabe BD, Fetter RD, Palmer JE, Hom S, Goodman CS (2003) Retrograde
771 control of synaptic transmission by postsynaptic CaMKII at the Drosophila neuromuscular
772 junction. Neuron, 39:255–267.
773
774 Halstead JM, Lin YQ, Durraine L, Hamilton RS, Ball G, Neely GG, Bellen HJ, Davis I (2014)
775 Syncrip/hnRNP Q influences synaptic transmission and regulates BMP signaling at the
776 Drosophila neuromuscular synapse. Biol Open, 3:839–849.
777
778 Haruna Y, Kobori A, Makiyama T, Yoshida H, Akao M, Doi T, Tsuji K, Ono S, Nishio Y,
779 Shimizu W, Inoue T, Murakami T, Tsuboi N, Yamanouchi H, Ushinohama H, Nakamura Y,
780 Yoshinaga M, Horigome H, Aizawa Y, Kita T, Horie M et al. (2007) Genotype-phenotype
781 correlations of KCNJ2 mutations in Japanese patients with Andersen-Tawil syndrome. Hum
782 Mutat, 28:208.
783
784 Haslbeck M, Weinkauf S, Buchner J (2019) Small heat shock proteins: Simplicity meets
785 complexity. J Biol Chem, 294:2121–2132.
786
787 Heginbotham L, Lu Z, Abramson T, MacKinnon R (1994) Mutations in the K^+ channel
788 signature sequence. Biophys J, 66:1061–1067.
789

790 Huang TH, Niesman P, Arasu D, Lee D, De La Cruz AL, Callejas A, Hong EJ, Lois C (2017)
791 Tracing neuronal circuits in transgenic animals by transneuronal control of transcription
792 (TRACT). Elife, 6:e26975.
793
794 Johns DC, Marx R, Mains RE, O'Rourke B, Marban E (1999) Inducible genetic suppression
795 of neuronal excitability. J Neurosci, 19:1691–7.
796
797 Joza N, Galindo K, Pospisilik JA, Benit P, Rangachari M, Kanitz EE, Nakashima Y, Neely
798 GG, Rustin P, Abrams JM, Kroemer G, Penninger JM (2008) The molecular archaeology of a
799 mitochondrial death effector: AIF in Drosophila. Cell Death Differ, 15:1009–1018.
800
801 Kazama H, Wilson RI (2008) Homeostatic matching and nonlinear amplification at identified
802 central synapses. Neuron, 58:401–413.
803
804 Kim D, Pertea G, Trapnell C, Pimentel H, Kelley R, Salzberg SL (2013) TopHat2: accurate
805 alignment of transcriptomes in the presence of insertions, deletions and gene fusions. Genome
806 Biol, 14:R36.
807
808 Kim SH, Ryan TA (2010) CDK5 serves as a major control point in neurotransmitter release.
809 Neuron, 67:797–809.
810
811 Koch I, Schwarz H, Beuchle D, Goellner B, Langegger M, Aberle H (2008) Drosophila
812 Ankyrin 2 is required for synaptic stability. Neuron, 58:210–222.
813
814 Kuypers HG, Ugolini G (1990) Viruses as transneuronal tracers. Trends Neurosci, 13:71–75.

Liu KS, Siebert M, Mertel S, Knoche E, Wegener S, Wichmann C, Matkovic T, Muhammad K, Depner H, Mettke C, Bückers J, Hell SW, Müller M, Davis GW, Schmitz D, Sigrist SJ (2011) RIM-binding protein, a central part of the active zone, is essential for neurotransmitter release. Science, 334:1565–1569.

Livak KJ, Schmittgen TD (2001) Analysis of relative gene expression data using real-time quantitative PCR and the $2^{-\Delta\Delta CT}$ method. Methods, 25:402–408.

Love MI, Huber W, Anders S (2014) Moderated estimation of fold change and dispersion for RNA-seq data with DESeq2. Genome Biol, 15:550.

Marie B, Pym E, Bergquist S, Davis GW (2010) Synaptic homeostasis is consolidated by the cell fate gene gooseberry, a Drosophila pax3/7 homolog. J Neurosci, 30:8071–8082.

McCabe BD, Hom S, Aberle H, Fetter RD, Marques G, Haerry TE, Wan H, O'Connor MB, Goodman CS, Haghighi AP (2004) Highwire regulates presynaptic BMP signaling essential for synaptic growth. Neuron, 41:891–905.

McDonald MJ, Rosbash M (2001) Microarray analysis and organization of circadian gene expression in Drosophila. Cell, 107:567–578.

McGuire SE, Le PT, Osborn AJ, Matsumoto K, Davis RL (2003) Spatiotemporal rescue of memory dysfunction in Drosophila. Science, 302:1765–1768.

840 Miesenböck G, Kevrekidis IG (2005) Optical imaging and control of genetically designated
841 neurons in functioning circuits. Annu Rev Neurosci, 28:533–563.
842
843 Morgan JI, Curran T (1991) Stimulus-transcription coupling in the nervous system:
844 involvement of the inducible proto-oncogenes fos and jun. Annu Rev Neurosci, 14:421–451.
845
846 Mosca TJ, Luo L (2014) Synaptic organization of the Drosophila antennal lobe and its
847 regulation by the Teneurins. eLife, 3:e03726.
848
849 Müller M, Liu KS, Sigrist SJ, Davis GW (2012) RIM controls homeostatic plasticity through
850 modulation of the readily-releasable vesicle pool. J Neurosci, 32:16574–16585.
851
852 Müller M, Pym EC, Tong A, Davis GW (2011) Rab3-GAP controls the progression of
853 synaptic homeostasis at a late stage of vesicle release. Neuron, 69:749–762.
854
855 Nitabach MN, Blau J, Holmes TC (2002) Electrical silencing of Drosophila pacemaker
856 neurons stops the free-running circadian clock. Cell, 109:485–495.
857
858 Paradis S, Sweeney ST, Davis GW (2001) Homeostatic control of presynaptic release is
859 triggered by postsynaptic membrane depolarization. Neuron, 30:737–749.
860
861 Petersen SA, Fetter RD, Noordermeer JN, Goodman CS, DiAntonio A (1997) Genetic
862 analysis of glutamate receptors in Drosophila reveals a retrograde signal regulating
863 presynaptic transmitter release. Neuron, 19:1237–1248.
864

865 Pfeiffer BD, Ngo T-TB, Hibbard KL, Murphy C, Jenett A, Truman JW, Rubin GM (2010)
866 Refinement of tools for targeted gene expression in Drosophila. Genetics, 186:735–755.
867
868 Pielage J, Cheng L, Fetter RD, Carlton PM, Sedat JW, Davis GW (2008) A presynaptic giant
869 ankyrin stabilizes the NMJ through regulation of presynaptic microtubules and transsynaptic
870 cell adhesion. Neuron, 58:195–209.
871 Quinn L, Coombe M, Mills K, Daish T, Colussi P, Kumar S, Richardson H (2003) Buffy, a
872 Drosophila Bcl-2 protein, has anti-apoptotic and cell cycle inhibitory functions. EMBO J,
873 22:3568–3579.
874
875 Renn SCP, Park JH, Rosbash M, Hall JC, Taghert PH (1999) A pdf neuropeptide gene
876 mutation and ablation of PDF neurons each cause severe abnormalities of behavioral
877 circadian rhythms in Drosophila. Cell, 99:791–802.
878
879 Ruda M, Coulter JD (1982) Axonal and transneuronal transport of wheat germ agglutinin
880 demonstrated by immunocytochemistry. Brain Res, 249:237–246.
881
882 Ruiz-Canada C, Ashley J, Moeckel-Cole S, Drier E, Yin J, Budnik V (2004) New synaptic
883 bouton formation is disrupted by misregulation of microtubule stability in aPKC mutants.
884 Neuron, 42:567–580.
885
886 Samuels BA, Hsueh YP, Shu T, Liang H, Tseng HC, Hong CJ, Su SC, Volker J, Neve RL,
887 Yue DT, Tsai LH (2007) Cdk5 promotes synaptogenesis by regulating the subcellular
888 distribution of the MAGUK family member CASK. Neuron, 56:823–837.
889

890 Sandrock AW, Dryer SE, Rosen KM, Gozani SN, Kramer R, Theill LE, Fischbach GD (1997)
891 Maintenance of acetylcholine receptor number by neuregulins at the neuromuscular junction
892 in vivo. Science, 276:599–603.
893
894 Schoch S, Castillo PE, Jo T, Mukherjee K, Geppert M, Wang Y, Schmitz F, Malenka RC,
895 Südhof TC (2002) RIM1alpha forms a protein scaffold for regulating neurotransmitter release
896 at the active zone. Nature, 415:321–326.
897
898 Schwab ME, Suda K, Thoenen H (1979) Selective retrograde transsynaptic transfer of a
899 protein, tetanus toxin, subsequent to its retrograde axonal transport. J Cell Biol, 82:798–810.
900
901 Scott K, Brady R, Cravchik A, Morozov P, Rzhetsky A, Zuker C, Axel R (2001) A
902 chemosensory gene family encoding candidate gustatory and olfactory receptors in
903 Drosophila. Cell, 104:661–673.
904
905 Seeburg DP, Feliu-Mojer M, Gaiottino J, Pak DT, Sheng M (2008) Critical role of CDK5 and
906 Polo-like kinase 2 in homeostatic synaptic plasticity during elevated activity. Neuron, 58:571–
907 583.
908
909 Sjulson L, Cassataro D, DasGupta S, Miesenböck G (2016) Cell-specific targeting of
910 genetically encoded tools for neuroscience. Annu Rev Genet, 50:571–594.
911
912 Söllner T, Whiteheart SW, Brunner M, Erdjument-Bromage H, Geromanos S, Tempst P,
913 Rothman JE (1993) SNAP receptors implicated in vesicle targeting and fusion. Nature,
914 362:318–324.

915

916 Stocker RF, Heimbeck G, Gendre N, de Belle JS (1997) Neuroblast ablation in Drosophila
917 P[GAL4] lines reveals origins of olfactory interneurons. J Neurobiol, 32:443–456.

918

919 Strack AM, Loewy AD (1990) Pseudorabies virus: a highly specific transneuronal cell body
920 marker in the sympathetic nervous system. J Neurosci, 10:2139–2147.

921

922 Sutcliffe B, Forero MG, Zhu B, Robinson IM, Hidalgo A (2013) Neuron-type specific
923 functions of DNT1, DNT2 and Spz at the Drosophila neuromuscular junction. PLoS ONE,
924 8:e75902.

925

926 Talay M, Richman EB, Snell NJ, Hartmann GG, Fisher JD, Sorkaç A, Santoyo JF, Chou-
927 Freed C, Nair N, Johnson M, Szymanski JR, Barnea G (2017) Transsynaptic mapping of
928 second-order taste neurons in flies by trans-Tango. Neuron, 96:783–795.e4.

929

930 Thiagarajan TC, Lindskog M, Tsien RW (2005) Adaptation to synaptic inactivity in
931 hippocampal neurons. Neuron, 47:725–737.

932

933 Trapnell C, Roberts A, Goff L, Pertea G, Kim D, Kelley DR, Pimentel H, Salzberg SL, Rinn
934 JL, Pachter L (2012) Differential gene and transcript expression analysis of RNA-seq
935 experiments with TopHat and Cufflinks. Nat Protoc, 7:562–578.

936

937 Tsurudome K, Tsang K, Liao EH, Ball R, Penney J, Yang JS, Elazzouzi F, He T, Chishti A,
938 Lnenicka G, Lai EC, Haghighi AP (2010) The Drosophila miR-310 cluster negatively
939 regulates synaptic strength at the neuromuscular junction. Neuron, 68:879–893.

Turrigiano G (2011) Too many cooks? Intrinsic and synaptic homeostatic mechanisms in cortical circuit refinement. Annu Rev Neurosci, 34:89–103.

Turrigiano G, Abbott LF, Marder E (1994) Activity-dependent changes in the intrinsic properties of cultured neurons. Science, 264:974–977.

Turrigiano GG, Leslie KR, Desai NS, Rutherford LC, Nelson SB (1998) Activity-dependent scaling of quantal amplitude in neocortical neurons. Nature, 391:892–896.

Valanne S, Wang J-H, Rämet M (2011) The Drosophila Toll signaling pathway. J Immunol, 186:649–656.

Vosshall LB, Amrein H, Morozov PS, Rzhetsky A, Axel R (1999) A spatial map of olfactory receptor expression in the Drosophila antenna. Cell, 96:725–736.

Wang HD, Kazemi-Esfarjani P, Benzer S (2004) Multiple-stress analysis for isolation of Drosophila longevity genes. Proc Natl Acad Sci U S A, 101:12610–12615.

Wang JZ, Du Z, Payattakool R, Yu PS, Chen CF (2007) A new method to measure the semantic similarity of GO terms. Bioinformatics, 23:1274–1281.

Wickersham IR, Lyon DC, Barnard RJO, Mori T, Finke S, Conzelmann K-K, Young JAT, Callaway EM (2007) Monosynaptic restriction of transsynaptic tracing from single, genetically targeted neurons. Neuron, 53:639–647.

965

966 Wierenga CJ, Ibata K, Turrigiano GG (2005) Postsynaptic expression of homeostatic

967 plasticity at neocortical synapses. J Neurosci, 25:2895–2905.

968

969 Yu XM, Gutman I, Mosca TJ, Iram T, Ozkan E, Garcia KC, Luo L, Schuldiner O (2013)

970 Plum, an immunoglobulin superfamily protein, regulates axon pruning by facilitating TGF-β

971 signaling. Neuron, 78:456–468.

972